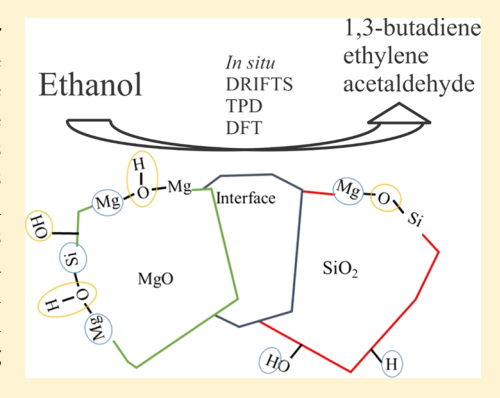


In Situ Spectroscopic Insights on the Molecular Structure of the MgO/SiO₂ Catalytic Active Sites during Ethanol Conversion to 1,3-**Butadiene**

William E. Taifan and Jonas Baltrusaitis*

Department of Chemical and Biomolecular Engineering, Lehigh University, B336 Iacocca Hall, 111 Research Drive, Bethlehem, Pennsylvania 18015, United States

ABSTRACT: Ethanol is an important renewable chemical that allows for sustainable high-value product, such as 1,3-butadiene, catalytic synthesis. The MgO/SiO₂ catalyst is typically utilized in a single-step ethanol-to-1,3-butadiene catalytic conversion, and the (by)product yields were shown to depend on the type, structure, and strength of the catalytic active sites. The fundamental factors describing the molecular structure and binding properties of these sites are thus of critical importance but not yet fully understood. We utilized a multimodal approach, including temperature-programmed surface-sensitive infrared mass spectrometry using probe molecules, such as CO₂, NH₃, and pyridine and propionic acids, to unravel the structure and persistence of these catalytic sites in situ. In particular, Mg-O-Mg, Mg-O(H)-Mg, Mg-O-Si, and Mg-O(H)-Si surface site binding configurations were proposed and scrutinized using spectroscopic methods in combination with density functional theory (DFT) calculations. A combination of NH3-temperature-programmed desorption and



DFT calculations allowed to better describe the molecular structure of said catalytic sites as the presence of open and closed Lewis acid sites (LASs) was suggested. The catalyst was shown to have both open LASs with both Mg_{3C} and Mg_{4C} as LASs and also very isolated closed LASs (Mg_{3C} and Mg_{4C}). Reactive molecule surface site poisoning experiments suggested that weak basic sites were responsible for ethanol dehydrogenation and strong basic sites were responsible for aldol condensation and Meerwein-Ponndorf-Verley reduction, whereas stronger acid sites catalyze acetaldol and crotyl alcohol dehydration reactions and weak acid sites catalyzed the undesired ethanol dehydration. In situ diffuse reflectance infrared spectroscopy and fixed-bed measurements indicated the consumption of the weak basic sites during the catalytic reaction. LASs were also consumed during the adsorption and the reaction and no generation of new basic sites was observed. The fundamental surface site structure proposed here can further serve as a starting point for theoretical calculations necessary to fully model the reactive pathway during ethanol catalytic transformation to 1,3-butadiene.

1. INTRODUCTION

Elucidating the surface active site molecular structure is of high importance for the development of selective MgO/SiO₂ catalysts utilized for the catalytic conversion of ethanol to 1,3-butadiene (1,3-BD). 1-4 The nature of the closed shell MgO electronic structure and diverse mixed oxide surface composition provide interesting analytical challenges as there are fewer spectroscopic methods that allow identification of the active site properties, akin to those for Ta₂O₅⁵ or ZrO₂, also used in ethanol-to-1,3-butadiene (ETB) catalytic conversion (1,3-BD).^{3,7} As a result, the surface site structure and the reactivity of MgO/SiO₂ catalysts during 1,3-BD production are still poorly understood.8 Selectivity differences between the catalysts often reported are due to the different active site densities, their functional nature (acidic or basic), and their strength which arise from the diverse set of preparation methods including the ratio of Mg-to-Si, Mg precursor used, and their deposition method. Catalysts prepared using different methods, for example, incipient wetness impregnation (IWI) and wet-kneading (WK),3,9 resulted in a large activity difference with the IWI-prepared catalyst yielding only ~5% conversion at 300 °C compared to the WK catalyst yielding ~50% conversion at 425 °C. A more appropriate comparison was done by He, et al., where differently prepared catalysts were tested using pulse-temperature-programmed desorption (TPD) method. 10 A comparison between IWI and WK catalysts showed that the IWI catalyst is more active in catalyzing dehydration than dehydrogenation reactions. This is further shown by the much higher 1,3-BD yield attained by the WK catalyst (73%) as compared to the IWI catalyst (45%) across the 50-500 °C temperature range. 10 This different activity was suggested to be due to the different silicate phase formation on the catalyst surface depending on the preparation technique.³ The ratio of acidic-to-basic sites was shown to also affect the overall reactivity during 1,3-BD formation, as demonstrated by Angelici et al. 9 Shylesh et al. proposed that

Received: July 15, 2018 Revised: August 16, 2018 Published: August 24, 2018



weak basic sites were responsible for ethanol dehydrogenation and other basic sites were responsible for aldol condensation.³ Angelici et al. attributed the higher overall reactivity to a small number of strong basic sites on the catalyst surface with an intermediate amount of acidic sites and weak basic sites. In general, MgO/SiO2 WK has consistently been shown to produce highest 1,3-BD yields 4,11,12 because of the proposed balanced acidic and basic catalytic site number.9

The exact molecular structure of these acidic and basic active sites is still under debate. 1,2,13 In particular, -Mg-O-Silinkage has been implicated to be reactive and related to the selectivity of the catalysts. ¹⁻³ SiO₂ was proposed to indirectly catalyze the reaction because of its structural perturbation of MgO using WK.11 Furthermore, a formation of a new phase of MgO with SiO₂ was inferred from the experimental measurements, and the amount of magnesium silicate phases, measured by ¹H-²⁹Si cross-polarized MAS NMR^{1,3} and diffuse reflectance infrared spectroscopy (DRIFTS),² was correlated with the overall selectivity. Velasquez Ochoa et al. observed the formation of a magnesium silicate phase with Mg²⁺ neighbored by Si⁴⁺ cations synthesized using sol-gel methods with Mg/Si ratio of 9-15, whereas the lower ratio led to the formation of a catalytically inactive forsterite (Mg₂SiO₄) phase.² Furthermore, the silicate-to-MgO ratio was suggested to be the key to the appropriate balance of acidic-basic sites. A different view was offered by Shylesh et al. where hydroxyl (OH) groups were necessary in the proximity of the strong basic $Mg^{2+} - O^{2-}$ sites to synergistically catalyze the reaction. Finally, the correlation between the magnesium silicate hydrous phase and 1,3-BD yield was challenged by Hayashi et al. who reported an active MgO catalyst that did not require participation from SiO₂. ¹³ Xray photoelectron spectroscopy characterization of the two different MgO catalysts, that is, with and without the additional hydrothermal step, showed that the latter, that is, the more active catalyst, exhibited a higher intensity of an unassigned O 1s oxygen peak at around 532 eV. 13 The presence of this unidentified oxygen species on MgO could be related to the reactive lower-coordinated oxygen atoms on Mg-O defect sites. 14-16 Concurrently, these lower-coordinated Mg-O pairs $({\rm Mg_{3C}}^{2+}{\rm O_{4C}}^{2-}, {\rm Mg_{3C}}^{2-}, {\rm O_{3C}}^{2-}, {\rm and} {\rm Mg_{4C}}^{2+}{\rm O_{4C}}^{2-})$ were computationally shown to be involved in 1,3-BD formation from ethanol.

Surface site study of MgO/SiO₂-based catalysts mostly concerns the general acidity and basicity characterization while also discussing the importance of silicate phases. 1,9,20,21 However, pyridine-DRIFTS studies concluded Lewis acid sites (LASs) to be the only acidic sites on the catalyst as demonstrated by the IR peaks at 1450, 1578, and 1612 cm⁻¹.3,9,20,21 NH₃-TPD, another routinely used acidity probe method, also discriminates the acid based on the strength, without discussing the nature of the acidic sites. Hence, the molecular structure of these acidic sites is not well known. In this work, we combined in situ spectroscopic measurements using different probe molecules to identify the role of each sites during the reaction and elucidate their molecular coordination. In particular, we begin by performing steadystate and kinetic temperature-programmed experiments of ethanol conversion to 1,3-BD using wet-kneaded catalysts. We then perform bulk X-ray diffraction (XRD), surface low-energy ion scattering (LEIS), and DRIFTS analysis of native surface hydroxyl groups. We then utilize temperature-programmed DRIFTS to explore surface acidic and basic site structures with ab initio calculations to support our NH₃ adsorption site

assignments and hence propose the molecular arrangements of the catalytic sites. Finally, the persistence of these reactive sites is probed spectroscopically under the relevant conditions of temperature and ethanol vapor.

2. EXPERIMENTAL METHOD

2.1. Catalyst Synthesis. The MgO/SiO₂ catalyst was prepared using a wet-kneaded method that was previously described.²² Briefly, the magnesium hydroxide material was prepared by thermal decomposition of the magnesium nitrate hexahydrate (Sigma) precursor in methanol. Magnesium hydroxide was wet-kneaded with fumed silica (Cabot) in deionized water, with liquid-to-solid volume ratio of 1, for 4 h. The final MgO/SiO₂ mass ratio of 1:1 was used for characterization and activity study. The resulting material was then dried overnight at 80 °C and then calcined at 800 °C. This catalyst is labeled as MgSi-WK. Several MgSi-WK catalysts with various ratios of Mg/Si were also synthesized, that is, Mg/Si of 1:10, 3:7, 7:3, and 10:1. The MgSi-WK2 catalyst was synthesized at Mg/Si = 1 and calcined at $500 \,^{\circ}$ C; the activity of this catalyst was tested and compared to the primarily studied catalyst, that is, MgSi-WK.

2.2. Steady-State Reactivity Testing. The steady-state catalytic tests were performed in a Microactivity-Reference fixed-bed reactor from PID Eng Tech (Spain). A quartz tube reactor was used with the quartz wool positioned to support the catalyst bed (0.1 g, pelletized, crushed, and sieved to 100-150 μ m particle size). Additional SiO₂ powder (Sigma) was used to increase the bed length to maintain the plug flow conditions. To demonstrate the inertness of SiO₂, a separate experiment (not shown) was performed to test the catalytic activity of bare SiO₂. The conversion achieved was very low, that is, up to 2%, with ethylene as the main product. On the basis of this finding, silica was assumed to not significantly modify the inherent activity of the studied catalysts. Ethanol was delivered using He gas by bubbling it through a chilled ethanol saturator with a total flow of 50 mL/min. The bubbler temperature was varied to manipulate the weight hourly space velocity (WHSV). The hot box temperature in the reactor was set at 100 °C to prevent any reactant or product condensation. Prior to the reaction, the catalyst was activated by heating it to 500 °C at a heating rate of 10 °C/min and holding it at that temperature for 1 h under a 30 mL/min He flow. The ethanol conversion reactions to 1,3-BD were performed at 375 °C. The products were kept in the vapor phase and then analyzed using a gas chromatograph equipped with a flame ionization detector and Restek RT-Q-Bond column. The reactant ethanol and principal (by)products, that is, ethylene, acetaldehyde, and 1,3-BD, were quantified based on the calibration carried out using a standard reference mixture (Praxair).

A reactive site titration experiment was carried out to reactively poison basic or acidic surface sites. To poison basic sites, probe molecules CO₂ and propionic acid were used. Poisoning of the acidic sites was carried out using NH3 as the probe molecule. In a typical titration experiment, the catalyst was allowed to achieve a steady-state condition at a selected WHSV and reaction temperature. The selected probe molecule was then cofed into the reactor using a mass flow controller for CO₂ and 1% NH₃ in N₂, whereas propionic acid was delivered using a chilled saturator containing a mixture of propionic acid/ethanol (3:7). After a new steady-state was achieved, the feed was reverted back to ethanol-only to investigate the recovery of the reactivity. The following definitions were used to describe the performance of the reactions:

Conversion

$$X_{\text{EtOH}}$$
 (%) = $\frac{n_{\text{EtOH,in}} - n_{\text{EtOH,out}}}{n_{\text{EtOH.in}}} \times 100$

Selectivity

$$S_i (\%) = \frac{n_i}{\sum n_i} \times 100$$

Productivity

$$P_i \text{ (mmol/g}_{cat} \text{ h}) = \frac{S_i \times X_{\text{EtOH}} \times n_{\text{EtOH,in}} \times 60}{\text{mass of catalyst (g)}} \times 1000$$

2.3. Catalyst Bulk and Surface Characterization. 2.3.1. Temperature-Programmed Surface Reaction—Mass Spectrometry. Temperature-programmed Surface Reactionmass Spectrometry (TPSR-MS was carried out using an Altamira Instruments system (AMI-200) connected to a DyMaxion Dycor mass spectrometer (DME200MS). Approximately 30 mg of the catalyst was loaded into a glass U-tube fixed-bed reactor and held in place by quartz wool. Prior to measurement, the catalyst was first pretreated under 10% O₂/ Ar (Airgas, certified, 9.99% O₂/Ar balance) at 500 °C for 1 h. After activation, the catalyst temperature was decreased to 100 °C. At this temperature, ethanol vapor was adsorbed for 15 min followed by degassing (purging) using Ar for 45 min. The vapor delivery system and procedure were used in the in situ DRIFTS experiments. The catalyst bed was heated at 10 °C/ min to 450 °C, and the evolution of the gas products was monitored with the online mass spectrometer. Acetaldehyde was delivered using a mixture of 5% acetaldehyde in N₂ (Praxair). A separate experiment involved preadsorbing acetaldehyde on the surface of the catalyst, followed by degassing with argon for 45 min and temperature increase at 10 °C/min to 450 °C under a constant ethanol/argon flow. The ethanol saturator temperature was held at 2 °C using an ice bath at all times. Table 1 shows the m/z utilized for reactive vapor (gas) species detection.

Table 1. m/z Selection to Identify the Arising Vapor-Phase Species from TPSR-MS Experiments

m/z	species
46	ethanol
26	ethylene
44	acetaldehyde
2	hydrogen
54	1,3-BD
70	crotonaldehyde
57	crotyl alcohol

2.3.2. XRD Analysis. Bulk structural information of MgSi-WK catalysts was obtained using XRD analysis. The XRD patterns were obtained using a PANalytical Empyrean powder X-ray diffractometer using Cu $K_{\alpha 1,2}$ with $\lambda=1.5418$ Å operating at 45 kV. The measurements were carried out between $2\theta=10^\circ$ and 100° using a step size of 0.05° .

2.3.3. Low-Energy Ion Scattering. LEIS is a surfacesensitive technique that allows for analyzing the chemical composition of the few topmost layers of the catalyst material.²³ During LEIS analysis, the sample surface is bombarded with noble gas ions at energy in the order of a few kiloelectron volts. The ions are backscattered by the atoms of the surface, and their energy is measured so the masses of the scattering surface atoms are determined. The measured intensity is directly proportional to the surface coverage of the corresponding element. The catalyst, that is, MgSi-WK, was prepared for surface elemental composition analysis by dispersing into a sample crucible, compacted with a sample press and mounted on a heatable sample holder within the LEIS spectrometer, ION-TOF Qtac¹⁰⁰. The crucible was then affixed to a sample holder with an integrated cartridge heater, and a thermocouple was placed into a hole on the crucible in the sample preparation chamber. After being evacuated, the temperature of the sample was raised to 50 °C for outgassing. O2 was then introduced into the chamber at a pressure of \sim 200 mbar. The temperature of the sample was then increased at a rate of 10 °C/min to a maximum temperature of 500 °C. This temperature was held for 60 min and allowed to naturally cool down to room temperature. The sample was then transferred into the analysis chamber. Charge neutralization was utilized during the spectra acquisition and depth profiling via sputtering. For the primary ion beam, the following parameters were used: 3.0 keV He⁺, 1500 \times 1500 μ m raster, at 2×10^{14} ions cm⁻² cyc⁻¹, 3000 eV pass energy. The following experimental conditions were used during sputtering: 1.0 keV Ar^{+} , 2000 × 2000 μ m raster, 5 × 10^{14} ions cm⁻² cyc⁻¹. Sputtering experiments (depth profiling) were carried out with the surface layers sputtered using 1 keV Ar+ ions. The sputtering rates were on the order of one monolayer of atoms per 10¹⁵ Ar⁺ ions cm⁻². For both Mg and Si, the peaks were fitted using Gaussian distributions with adjustable baseline heights on either side of the peak. O peaks, on the other hand, were integrated assuming a linear background. All peak fitting and background subtraction were performed using CasaXPS

2.3.4. Diffuse Reflectance Infrared Spectroscopy. The nature of the hydroxyl (OH) group composition on the catalyst surface under dehydrated conditions was studied using DRIFTS. A Thermo Nicolet iS50 infrared spectrometer equipped with a mercury-cadmium-tellurium liquid nitrogen-cooled detector was used in combination with a Harrick Praying Mantis diffuse reflection accessory equipped with ZnSe windows. About 30 mg of the <100 μ m catalyst was loaded into the DRIFTS cell. The smaller particle size was used to ensure a uniform catalyst bed surface for spectroscopy. Prior to analysis, the catalyst was activated by heating it up to 500 °C at 10 °C/min and holding it at that temperature for 1 h under a 30 mL/min air flow. The catalyst was then cooled down to 100 °C under a 30 mL/min N₂ (Praxair) flow. During the cooling, reference spectra of the catalysts were acquired at 400, 300, 200, and 100 °C. All spectra were averaged over 96 scans at a resolution of 4 cm⁻¹.

Acidity and basicity of the catalysts were characterized using temperature-programmed adsorption of probe molecules, including pyridine, NH_3 , and CO_2 . After the sample surface activation, the selected probe molecule was adsorbed on the surface for 15 min at 100 °C. This step was followed by purging using 30 mL/min N_2 (Praxair) for 45 min. Spectra were continuously recorded every minute concomitantly with the temperature increase to 450 °C under a 30 mL/min N_2 flow. CO_2 and NH_3 (Praxair) gases were delivered from the pressurized gas tank using mass flow meters, whereas the pyridine delivery method involved saturating N_2 using a

pyridine saturator. The catalyst acidity and basicity after ethanol adsorption at 100 $^{\circ}$ C and after reaction with ethanol at 200 $^{\circ}$ C were investigated to elucidate the role and the fate of each site in situ. In the first experiment, ethanol was adsorbed at 100 $^{\circ}$ C for 20 min, flushed with an inert gas for 1 h, and the resulting surface sites were probed with CO₂ or pyridine in situ. In the second experiment, the reaction with ethanol was carried out at 200 $^{\circ}$ C to initiate ethanol dehydrogenation. After 1 h of reaction, the reaction cell was flushed and CO₂ or pyridine was introduced into the cell.

2.4. Quantum Chemical Calculations. 2.4.1. Molecular Structure of the Catalytic Site. Analysis of Lewis acid ZrO2based catalysts²⁵ suggests that LASs can be chiefly responsible for the activity in this reaction. By definition, closed Lewis acid heteroatoms (M) are tetrahedrally coordinated $(M-(OSi)_4)$ to the zeolite framework, whereas open Lewis acid heteroatoms are tricoordinated (HO)-M-(OSi)₃ to the zeolite framework. 26-28 With this in mind, the octahedral symmetry in the MgO crystal^{13,29} allows us to identify several LASs as part of the intrinsic acid-base pairs to be available, that is, Mg-O-Mg, Mg-O(H)-Mg, Mg-O-Si, and Mg-O(H)-Si. These combinations can further exist in open and closed acid configurations, where oxygen is bound to SiO2 while also coordinated to a proton to form coordinated hydroxyl groups. 30,31 The strict terminology of the open acid site requires an isolated hydroxyl group to be present, and while it is very basic, this hydroxyl group has been proven to be nonexistent spectroscopically. ^{31,32} In addition to these sites, the coordination of Mg is also very important because catalysis by this metal oxide is driven by defect sites. 16,33,34 These proposed Mg atoms constituting the catalytic sites are shown in Figure 1.

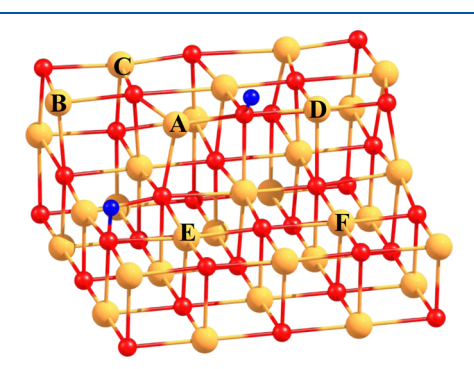


Figure 1. Possible combination of metal atoms that act as LAS: (A) Mg_{3C} (open), (B) Mg_{3C} (closed), (C) Mg_{4C} (closed), (D) Mg_{4C} (open), (E) Mg_{5C} (open), and (F) Mg_{5C} (closed).

2.4.2. Structural Optimization and Frequency Calculations. These sites were modeled using a periodic three-layer slab of MgO consisting of $8 \times 6 \times 3$ primitive cells used throughout all of the calculations. Previous investigations have identified defect sites of MgO catalysts, most notably the three-and fourfold coordinated surface atoms $({\rm Mg_{3C}}^{2+}{\rm O_{4C}}^{2-})$, as the active sites, 14,16,29,30,34,35 whereas atoms at surface terraces were found to be relatively unreactive. The positions of atoms in the bottommost layer were fixed, whereas remaining atoms were relaxed. A Perdew–Burke–Ernzerhof (PBE) lattice parameter of 4.255 Å was used to construct the slab. This value is similar to the values of 4.261 (PBE) and 4.186 Å (experimental). During the optimization, the bottom layer was not optimized to replicate bulk of the catalyst. Periodic

density functional theory (DFT) calculations have been performed using the VASP code. ^{38–41} The Kohn–Sham equations have been solved variationally in a plane-wave basis set using the projector-augmented-wave method of Blöchl, 42 as adapted by Kresse and Joubert. 42 The exchange-correlation energy was described by the PBE generalized gradient approximation. 43 Brillouin zone was sampled using a $2 \times 2 \times 1$ k-point mesh. The plane-wave cutoff was set to 400 eV. The convergence criterion for the electronic self-consistency cycle, measured by the change in the total energy between successive iterations, was set to 10^{-6} eV/cell. Atomic positions were considered to be relaxed if all forces acting on the atoms were smaller than 0.005 eV/Å. Frequency calculations were performed for NH₃ infrared spectra analysis. A scaling factor of 0.9854 was applied to the calculated values and was derived from the gas-phase NH3 experimental and DFT-calculated frequencies.

3. EXPERIMENTAL RESULTS

3.1. Steady-State Ethanol Catalytic Conversion to 1,3-BD. Steady-state reactivity of MgO/SiO₂ catalysts was investigated using a fixed-bed reactor at 450 °C. At this reaction temperature, the carbon balance was determined to be >80%. The catalyst calcination temperature affected the reaction product distribution. Table 2 shows that ethylene

Table 2. Steady-State Reactivity of ${\rm MgO/SiO_2}$ Catalysts of Different Calcination Temperatures

		selectivity (%)			
catalyst	ethylene	acetaldehyde	1,3-BD	conversion (%)	
MgSi-WK (calcined at 800 °C)	55.8	14.4	29.7	77.0	
MgSi-WK2 (calcined at 500 °C)	82.9	9.7	7.5	60.4	

"Reaction was carried out at 450 °C with catalyst mass of 0.1 g, 55 mL/min total flow rate, and $p_{\rm ethanol}$ = 2.5 kPa. The selectivity toward major (by)products ethylene, acetaldehyde, and 1,3-BD is reported. TOS = 50 min.

selectivity was the highest for MgSi-WK2, which suggests the presence of acidic sites on the surface because the ethanol dehydration reaction is very prominent over catalysts with very high density of Brønsted acid sites (BASs). 44-46 The selectivity toward the products over basic sites, that is, acetaldehyde and 1,3-BD (vide infra), was higher for MgSi-WK, further emphasizing the increased number and availability of the acidic sites on the catalyst surface when it was calcined at lower temperature. The ethylene selectivity for MgSi-WK was, however, still above 50%, which is intriguing, because the acid sites found in the catalyst are primarily LASs (vide infra). This suggested that the BASs are not the only sites responsible for the dehydration of ethanol to ethylene.

Figure 2 shows the evolution of each major (by)product with increasing temperature for the reaction over the MgSi-WK catalyst. 1,3-BD and ethylene exhibited an almost linear increase in productivity with the calculated apparent activation energies of 12.4 and 18.02 kcal/mol, respectively. Productivity values of MgSi-WK compared reasonably well with those found in the literature. In the present work, 1,3-BD yield translated to the production rate of 0.44 g_{BD}·g_{cat}⁻¹·h⁻¹, whereas MgSi-WK2 yielded about 0.06 g_{BD}·g_{cat}⁻¹·h⁻¹. Chung et al. synthesized a WK catalyst using a calcination temperature of

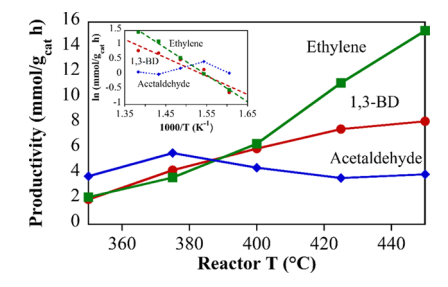


Figure 2. Catalytic activity of MgSi-WK between 350 and 450 $^{\circ}$ C. Inset: Arrhenius plot of ethylene and 1,3-BD. Catalyst mass = 0.1 g, total flow rate = 55 mL/min, $p_{\rm ethanol}$ = 2.5 kPa.

500 °C with the reported 1,3-BD productivity of 0.23 g_{BD} · g_{cat}^{-1} ·h⁻¹. The origin of this reactivity can be traced to the high amount of the proposed layered hydrous magnesium silicate phase on the catalyst, which was highly dependent on the precursor; a nanosized $Mg(OH)_2$ precursor was the preferred precursor. The effect of the MgO precursor used during the WK catalyst synthesis has recently been highlighted by Huang et al. where the $Mg(OH)_2$ precursor synthesized using a templated method yielded a very high productivity of 1.15 g_{BD} · g_{cat}^{-1} ·h⁻¹.

3.2. TPSR-MS of Ethanol on MgSi-WK. To understand the reaction mechanism, TPSR-MS was carried out using the ethanol reactant and intermediate reactive molecules. TPSR-MS provides vapor-phase analysis which allows one to understand the mechanism as a prelude to the analysis of the catalytic sites involved. The TPSR-MS experiment was performed under a constant ethanol feed flow and shown in Figure 3a. The ethanol signal continuously decreased during the reaction as a function of temperature without the presence of any products detected. This is consistent with the previous report, where a significant amount of reactive intermediates was bound strongly to the catalyst surface.²² Ethylene was the first product to be detected at ~200 °C, which can be explained by the lower desorption energy of ethylene than that of acetaldehyde.¹⁷ Acetaldehyde, when formed, tends to remain on the surface to undergo several other surface reactions, such as aldol condensation and polymerization.² The more significant consumption of ethanol took place at 300 °C, where acetaldehyde and hydrogen were detected, which can be explained by the accelerated dehydrogenation reaction. Very low signals of crotyl alcohol and crotonaldehyde were also evident from the spectra, which indicated the tendency of these species to undergo a surface reaction rather than to desorb off the surface.

Evolution of the reactive intermediates and byproducts during the acetaldehyde temperature-programmed experiment is shown in Figure 3b. Crotonaldehyde was formed which is in good agreement with DRIFTS experiments reported previously. Several desorption peaks were observed at 210, 330, and 410 °C (acetaldehyde) and 210, 350, and 422 °C (crotonaldehyde). Second peaks at 330 and 350 °C for acetaldehyde and crotonaldehyde, respectively, indicated that a secondary reaction was taking place. As previously suggested, the accumulation of acetaldehyde on the catalyst surface will lead to aldol condensation between crotonaldehyde and acetaldehyde to yield 2,4-hexadienal. This reaction was confirmed by the change of slope from the water signal m/z=18, which increased when the other signals decreased.

TPSR-MS experiments were conducted with both ethanol and acetaldehyde (Figure 4). This experiment mimics a two-

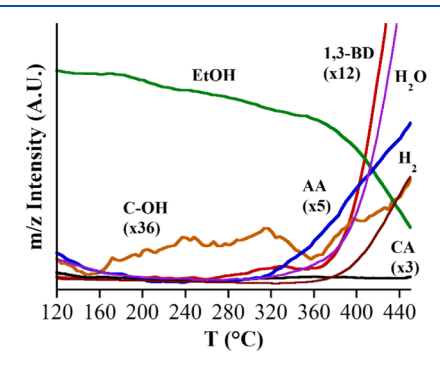


Figure 4. TPRS spectra of the ETB reaction over MgSi-WK with ethanol and acetaldehyde as the coreactants. Acetaldehyde is preadsorbed on the surface and temperature ramp is under ethanol.

step reactive process where acetaldehyde is cofed with ethanol. If acetaldehyde production is the rate-determining step, any accumulation of acetaldehyde on the surface would increase 1,3-BD production. This experiment did not increase the production of 1,3-BD as one would expect ethanol to immediately undergo Meerwein—Ponndorf—Verley (MPV) reduction with the produced crotonaldehyde on the surface. Rather, 1,3-BD production was low until 360 °C, which is much later for ethanol alone. The sudden increase of the 1,3-BD production was accompanied by water production, which suggested that the dehydration of crotyl alcohol was lagging until 360 °C.

3.3. Bulk, Surface Chemical, and Structural Characterization Using XRD, LEIS, and DRIFTS. Bulk crystalline structures of the catalysts were characterized using XRD. The

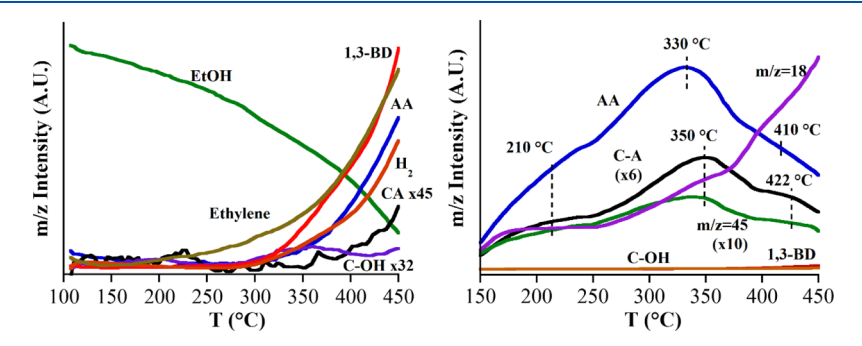


Figure 3. TPSR-MS spectra of the ETB reaction over MgSi-WK with ethanol as the feed (left) and acetaldehyde as the feed (right). EtOH: ethanol; AA: acetaldehyde; CA: crotonaldehyde; C-OH: crotyl alcohol.

XRD patterns of the selected MgSi-WK catalysts as a function of the corresponding oxide ratio are compared in Figure 5. The

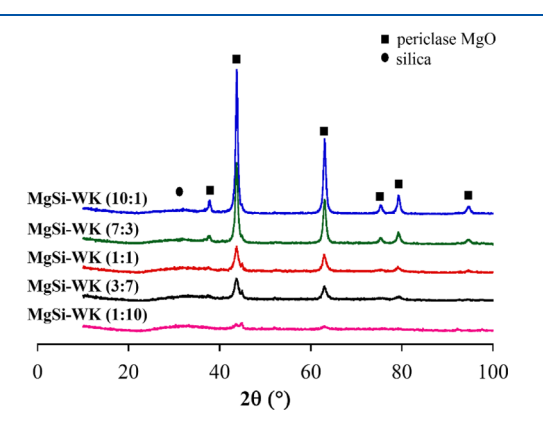


Figure 5. XRD patterns of MgSi-WK with different oxide ratios.

XRD pattern of WK catalysts indicates the formation of periclase MgO in the bulk. The intensity increased with higher Mg content, which means that the catalyst crystallinity originated from MgO rather than any silicate material. The presence of the amorphous feature on the XRD patterns due to SiO_2 for all catalysts further indicated that the high calcination temperature did not change the crystallinity of SiO_2 .

The topmost surface layer of the catalysts was probed using LEIS. 23 The LEIS spectra of both catalysts are shown in Figure 6. The legend in the inset in Figure 6, left indicates that the nth atomic layer is removed from the catalyst surface. Three peaks were found in the spectra corresponding to oxygen at \sim 1200 eV, Mg at \sim 1650 eV, and a shoulder for Si at \sim 1760 eV. The increase in signal intensity for all peaks after initial sputtering may be due to initial planarization of the catalyst granules increasing the apparent global atomic surface density. The resulting depth profile demonstrated the Si-rich surface of MgSi-WK. This suggests that the WK method provided intimate mixing between Mg(OH) $_2$ and SiO $_2$ allowing for the extensive interaction between the two oxides, which is reflected in the abundance of Si on the surface.

The structure of the native OH groups of all of the catalysts was investigated using DRIFTS and shown in Figure 7. There are four major peaks in the spectrum in addition to a broad peak at $\sim 3550~\rm cm^{-1}$ assigned to germinal and vicinal OH groups of the silica support. The peak at 3745 cm⁻¹ was assigned to both isolated silanol groups of the SiO₂ support, which decreased in intensity when MgO was wet-kneaded, and to an isolated OH group of MgO that

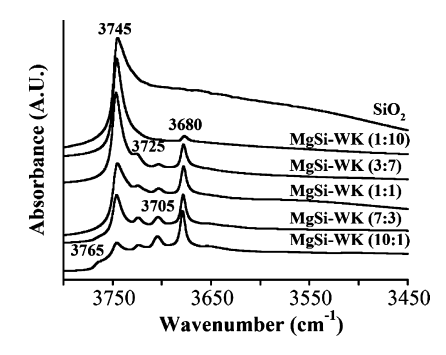


Figure 7. OH groups of WK catalysts with different oxide ratios as compared using DRIFTS.

depends on the coordination number of Mg.²² An intense peak at 3680 cm⁻¹ was previously assigned to a magnesium silicate phase, lizardite. The other peaks at 3725 and 3705 cm⁻¹ were assigned to the isolated O_{4c}-H and O_{5c}-H coordinated groups formed in the presence of amorphous SiO₂ (SiMg_{4c}O_{4c} and SiMg_{4c}O_{5c}), respectively. ²² Formation of the peaks at 3725 and 3705 cm⁻¹ was also confirmed with varying Mg/Si ratios. At very high Mg content, that is, Mg/Si > 7:3, it can be seen that a very basic Mg-OH group started to become apparent at 3765 cm⁻¹. As previously shown, ²² MgO possessed two basic OH groups that depend on the coordination number of oxygen atoms with the lower coordinated OH group at higher wavenumbers. 31,50 Interestingly, the peaks at 3705 and 3680 cm⁻¹ increased with the Mg content, whereas the peak at 3725 cm⁻¹ intensified at an intermediate ratio and diminished at both extremes.

3.4. Acid-Base Property and Molecular Structure Characterization of the Active Sites Using DRIFTS. The acidity and basicity of the catalysts were investigated using CO_2 , NH_3 , and pyridine as probe molecules and shown in Figure 8. CO_2 adsorbs on basic surface sites as surface carbonate and bicarbonate species. The formation of these surface species can be associated with the strength of the corresponding basic sites. Adsorption of CO_2 on MgSi-WK resulted in three major, broad peaks at 1655, 1541, and 1406 cm⁻¹. These peaks dramatically decrease in intensity when the temperature was increased up to 450 °C. At this temperature, only some peaks remained, that is, the bands at \sim 1600 and \sim 1400 cm⁻¹. These bands indicate the presence of a strongly-bound CO_2 species at this high temperature.

Pyridine is a weak base and can discriminate between LASs and BASs, although its use is limited by its relatively large molecule size in comparison to NH₃. Pyridine adsorbs on a

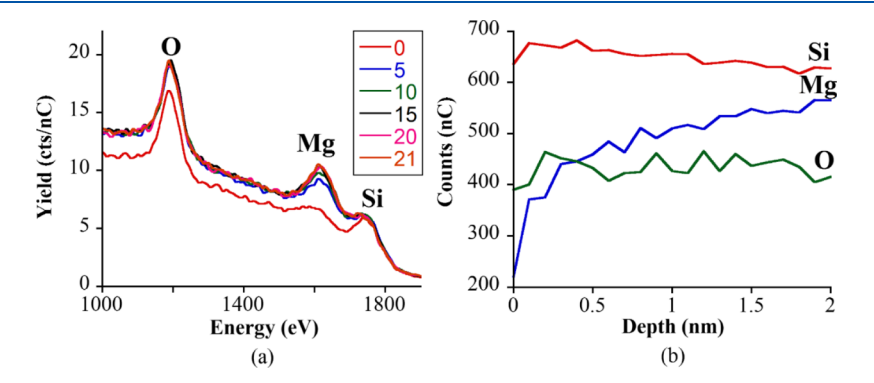


Figure 6. (left) HS-LEIS spectra of layer-by-layer sputtering of the MgSi-WK surface. (right) Depth profile of MgSi-WK as probed using HS-LEIS.

The Journal of Physical Chemistry C

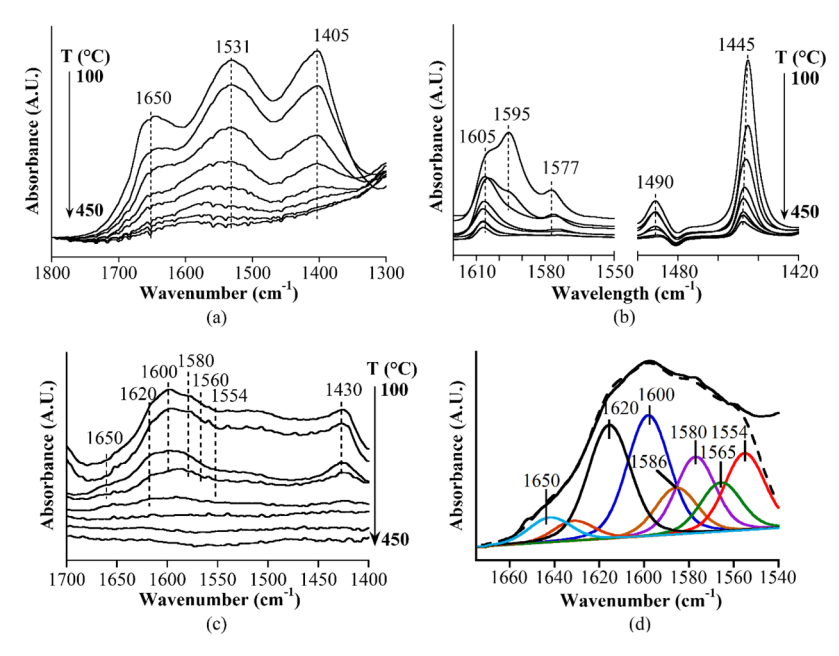


Figure 8. Acid—base characterization of the MgSi-WK catalyst probed using CO₂ (a), pyridine (b), and NH₃ (c). Deconvolution of the DRIFTS spectra of the NH₃ surface species on the catalyst showed differently coordinated species (d). TPD experiments using DRIFTS are shown. The background spectra of the pretreated catalyst were subtracted from the original spectra to exclusively show contributions from the adsorbed molecules.

catalyst surface as a physisorbed molecule, Lewis-bonded species, and as pyridinium ions. ^{52–54} Observation of the latter two species allows for the discrimination between the LASs and BASs. ⁵⁵ BASs, which would be indicated by peaks at 1638 and 1540 cm⁻¹, ⁵⁵ were not observed in agreement with the observations of Angelici et al. and Janssens et al. ^{9,20} The catalyst exhibited a similar Lewis acidity as shown at 450 °C as evident from the peaks at 1445, 1590, and 1605 cm⁻¹. The peaks at 1445 and 1608 cm⁻¹ shifted to 1450 and 1608 cm⁻¹, respectively, at higher temperature, that is, 450 °C, whereas the peak at 1490 cm⁻¹, which is a combination band of both LASs and BASs, disappeared. The origin of this Lewis acidity is from electron-deficient Mg atoms in the Mg–O–Si coordination and Mg–O–Mg coordination. ^{13,30,34,35}

Figure 8c depicts the acidity probing using NH₃-TPD IR. To aid assignments, these peaks were deconvoluted using CasaXPS.²⁴ Several peaks assignable to NH₄⁺ and NH₃-Lewis bound species appeared on the spectra, that is, at 1650 (very weak), 1620 (strong), 1600 (strong), 1586 (weak), 1580 (strong), 1560 (weak), 1540 (moderate), and 1430 cm⁻¹ (strong). These peaks gradually decreased with the increasing catalyst temperature. The peaks in 1620-1550 cm⁻¹ more prominently decreased, indicating the weak nature of these acid sites. This convoluted nature of the peaks/bands formed during NH₂ exposure was often cited as the main limiting factor of NH₃ as a probe molecule. 56 However, one noticeable difference from the two spectra groups shown, that is, Figure 8b,c, is the presence of BASs on the NH₃ experiment, indicated by the peak at 1430 cm⁻¹. This was attributed to the small size of NH3 that could penetrate smaller pores in the catalyst structure.9 The peaks that were assignable to LASs were measured at 1560, 1580, 1586, 1600, 1620, and 1650 cm⁻¹. To aid the assignments of these peaks, DFT vibrational frequency calculations were performed on the defect sites of MgO, that is, Mg_{3C}O_{4C} and Mg_{4C}O_{4C} for both open and closed LASs

(Figure 9). The corresponding vibrations are tabulated in Table 3.

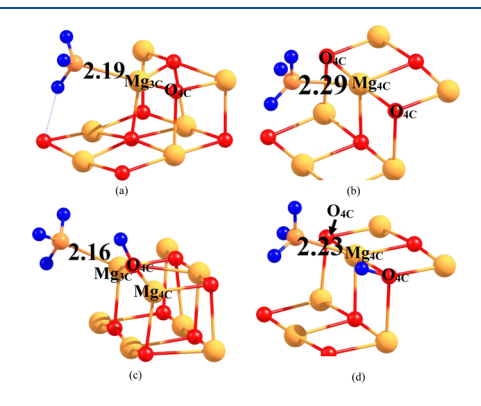


Figure 9. (a) Mg_{3C}, closed, (b) Mg_{4C}, closed, (c) Mg_{3C}, open, and (d) Mg_{4C}, open. Multiple possible adsorption sites, that is, kink (Mg_{3C}O_{4C}), edge (Mg_{4C}O_{4C}), and planar (Mg_{5C}O_{5C}) are highlighted.

Assuming an ideal surface and a similar trend on Mg-O-Si sites, peak assignments can be readily made. Closed LASs were

Table 3. Comparison between Observed Experimental Values of NH₃ Adsorption on MgSi-WK Catalysts with DFT-Calculated IR Vibrations of NH₃ Adsorbed on Open and Closed Acid Mg_{3C} and Mg_{4C} Sites

		calculated vibrational mode		experimer	ntal values
type	Mg coordination	δ_{as} H-N-H	$\delta_{\rm s}$ H-N-H	δ_{as} H-N-H	$\delta_{\rm s}$ H-N-H
open	4C	1592	1566	1600	1560
	3C	1574	1534	1570	1540
closed	4C	1588	1571	1586	N/A
	3C	1620	1577	1620	1580

The Journal of Physical Chemistry C

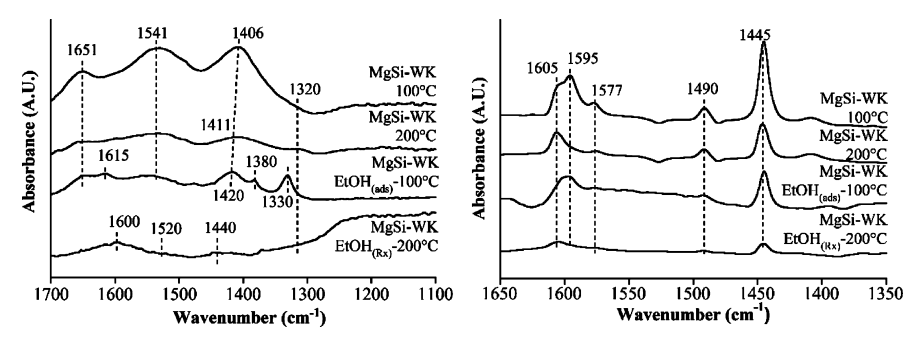


Figure 10. In situ acid—base characterization of the MgSi-WK catalyst before and after ethanol adsorption at 100 $^{\circ}$ C and reaction at 200 $^{\circ}$ C using CO₂ (left) and pyridine (right).

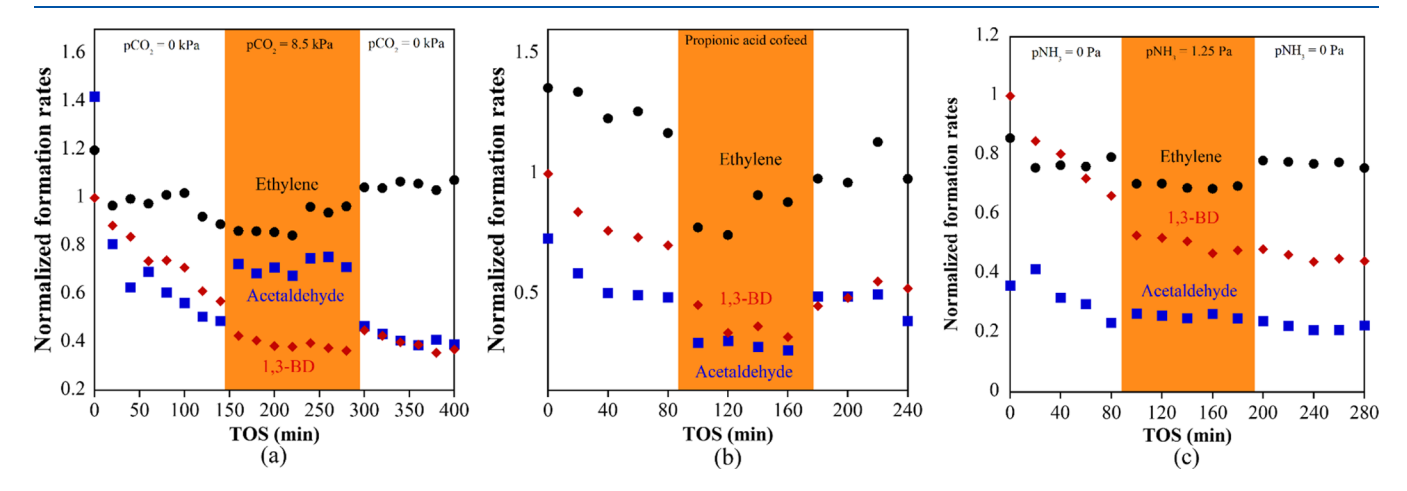


Figure 11. Acid—base poisoning reactivity testing using (a) CO_2 , (b) propionic acid, and (c) NH_3 to determine the role of each site during ethanol conversion to 1,3-BD over the WK-800 MgO/SiO₂ catalyst. The reactions are carried out at 425 °C, $m_{cat} = 0.1$ g, $p_{ethanol} = 2.5$ kPa, total flow = 55 mL/min. All formation rates are normalized to the initial 1,3-BD formation rate.

evident from the peaks at 1620 and 1580 cm⁻¹ (Mg_{3C}), whereas open LASs from Mg_{4C} were recognized by peaks at 1600 and 1560 cm⁻¹. Additionally, a closed LAS with 4C configuration was also observed, signified by the presence of a peak at 1586 cm⁻¹, although the corresponding symmetrical stretch was not visible. The presence of a peak at 1540 cm⁻¹ signified the presence of another open LAS (Mg_{3C}), which would be accompanied by a shoulder peak at ~1570 cm⁻¹.

3.5. Reactive Site Persistence during the ETB Catalytic Reaction. To elucidate the role of the specific basic and acidic sites during the reaction on the aged catalyst, in situ characterization experiments were performed using CO₂ and pyridine after the ethanol reaction on MgSi-WK. The catalyst surface was exposed to ethanol at 100 °C or reacted at 200 °C. Figure 10 (left) shows the spectra resulting from CO₂ adsorption on these aged samples. Three distinct peaks at 1615, 1380, and 1330 cm⁻¹ appeared on the catalyst that was previously exposed to ethanol (MgSi-WK EtOH(ads)) at 100 °C that do not originate from CO₂. While peaks at 1380 and 1330 cm⁻¹ were assigned to $\rho_{\rm w}$ (CH) and $\rho_{\rm w}$ (CH₃) of surface ethoxide, respectively,²² a peak at 1615 cm⁻¹ can be associated with a monodentate carbonate, accompanied by the symmetrical vibration peak at ~1320 cm⁻¹. After ethanol adsorption, all peaks decreased in intensity, as compared to CO₂-only adsorption on the unreacted catalyst at the same temperature. This decrease indicates a competitive adsorption between ethanol and CO₂ that resulted in surface ethoxide and both monodentate and bidentate carbonate. This indicates that ethanol preferably adsorbed on the strong basic sites that

would form monodentate and bidentate carbonate when exposed to CO2. The reaction at 200 °C was performed in situ before degassing with inert and adsorption of CO₂. The reaction temperature of 200 °C was chosen to limit further reactions to 1,3-BD. Extensive inert degassing was done to limit the further C4 oxygenates formed from facile aldol condensation, dehydration, and polymerization from occupying the site.²² A comparison of the spectra between CO₂ adsorbed on the activated catalyst and aged catalyst, that is, extensively reacted at 200 °C, showed a decrease in intensity on all peaks related to all surface species arising from CO₂. Weak basic sites, which are represented by peaks at ~1650 and ~1400 cm⁻¹ (surface bicarbonate),⁵⁷ were depleted. This indicates the consumption of the weak basic sites during the reaction. These weak basic sites result from MgO/SiO2-OH groups because the strong Mg²⁺-O²⁻ pairs form monodentate and bidentate carbonate when exposed to CO2. 34 Pyridine probing of the acidic sites shows a nondiscriminative trend for both ethanol adsorption at 100 °C and reaction at 200 °C. LASs were indeed consumed during the adsorption and even more so after the reaction at 200 °C, as indicated in Figure 10 (right). No generation of new BASs was observed after either adsorption or reaction as indicated by the absence of peaks at 1545 and 1638 cm^{-1.55} This suggested that the Mg-O-Mg linkages present on MgO exhibits Lewis acidity to a certain extent, which is responsible for both ethanol adsorption and reactions. In addition to the strong basicity that was also exhibited by the same linkage through the CO₂ adsorption experiment, it could be deduced that this linkage is providing both strong basic-weak acid Lewis pairs.

To further elucidate the role of acidic and basic sites during the reaction to 1,3-BD, surface site poisoning experiments were carried out using probe molecules such as CO₂, propionic acid, and NH3 in a steady-state fixed-bed reactor. CO2 and propionic acid are two weak acids, whereas NH3 is a basic probe molecule. Figure 11a shows the effect of cofeeding with CO₂. A slow, steady decrease in acetaldehyde and 1,3-BD production before CO2 was introduced, which indicates slow catalyst deactivation. However, once CO2 was cofed to the system, the formation rate of 1,3-BD and ethylene dropped, whereas acetaldehyde production increased. CO2 is a weaker acid than propionic acid and will bind to the strongest basic sites. This poisoning effect suggests that CO2 poisoned the sites that catalyzed aldol condensation and the subsequent steps because more acetaldehyde was released into the vapor phase without further reacting. When CO2 flow was switched off, the production of acetaldehyde, 1,3-BD, and ethylene was restored, confirming the weak interaction between CO2 and the strong basic sites.

Figure 11b shows product formation rates upon the introduction of propionic acid. All three products showed a decline in the formation rate. When propionic acid concurrent flow was stopped, the production of acetaldehyde was restored but 1,3-BD and ethylene formation did not recover. Propionic acid interacted more strongly with the stronger base sites but also binds to any weaker basic sites. Hence, when propionic acid flow was stopped, only weak basic sites were accessible, whereas some of the strong basic sites were permanently poisoned. From the two experiments, it is evident that acetaldehyde production was catalyzed by weak basic sites and 1,3-BD production was catalyzed by strong basic sites. The production of acetaldehyde over the weak basic site is consistent with the DRIFTS performed using CO2 as a probe molecule. A similar phenomenon was observed by Shylesh, et al. where the 1,3-BD formation rate did not recover during propionic acid cofeeding experiment over the Aupromoted IWI MgO/SiO₂ catalyst.³ Very interestingly, ethylene formation during the cofeeding experiments followed the trend of 1,3-BD. As previously suggested, ethylene formation can be carried out over both Lewis acidic Mg atoms (LASs) in the Mg-O-Mg or Mg-O-Si sites and the acidic O-H group (BASs). 17,58 Poisoning with both CO2 and propionic acid affected the strong Lewis basic pair, that is, oxygen anions, which inevitably perturbed the strong and medium Lewis acid Mg atoms in Mg-O-Mg and Mg-O-Si as well.

NH₃ is a relatively strong gas-phase base, stronger than pyridine and other organic basic molecules, such as acetonitrile and benzenes. 52 At the reaction temperature of 425 °C, NH₃ exhibits very weak adsorption on the surface and would interact with the acidic sites. Evident from Figure 11c, acetaldehyde production was hardly affected by the poisoning, as opposed to 1,3-BD and ethylene, where the decrease in production was more pronounced. While ethylene formation inhibition was reversible, 1,3-BD formation was irreversibly affected. NH3 poisoned both strong and weak BASs and LASs, but when its flow was discontinued, only the strong BASs were poisoned. The ethylene synthesis trend was very similar for both propionic acid and NH3 cofeeding, which indicates the same acid-base pairs being poisoned during the experiment. 1,3-BD production involves two dehydration steps, and the poisoning indicates that its production did not require

participation from the site that dehydrates ethylene. From these experiments, it is evident that the dehydration steps of both acetaldol and crotyl alcohol were catalyzed by strong acidic sites, whereas ethanol dehydration was catalyzed by weaker acidic sites.

4. DISCUSSION

4.1. Mechanistic Insights of 1,3-BD Formation from **Ethanol.** The activity comparison of the two catalysts showed that the catalyst calcined at 800 °C is more active than the one calcined at 500 °C. An earlier study by Zhu et al. reported that 500 °C was the optimized calcination temperature that resulted in balanced acidic-basic sites at 40.8 μ mol/g versus 49 μ mol/g.⁵⁹ The current finding, however, contradicts that of Zhu et al., which suggested that the catalyst calcined at 500 °C yielded a balanced acidic-basic site. 59' This discrepancy is possibly attributed to the use of pyridine to quantify the acidity of the catalyst because it had been shown that pyridine cannot penetrate smaller pores within the catalyst because of its bulk structure.⁹ This is also supported by our acidity testing experiments where the NH3 test showed that the catalyst possessed BASs, a result not shared by the pyridine test. The improvement of 1,3-BD formation from increasing the calcination temperature was followed by the significant decline of ethylene production. However, although the decrease was noticeable, ethylene still formed with ~50% selectivity. Ethanol dehydration typically proceeds on acidic catalyst sites. A set of experiments done by Badlani and Wachs using methanol over the individual components of the used catalysts, that is, MgO and SiO2, did not indicate extensive formation of dimethyl ether. 60 This suggested that BASs are not the only sites contributing to ethanol dehydration to ethylene. Previous work suggested that ethylene formed because of the reactive Mg-O-Mg or Mg-O-Si linkages that are intrinsic in WK catalysts. 17,22 The significant suppression in the formation of ethylene was further highlighted by the activation energy analysis. Analysis of the activation energy shows that ethylene (18.02 kcal/mol) is more sensitive to the increase in temperature, as opposed to 1,3-BD (12.4 kcal/mol). This suggested that lowering the reaction temperature might benefit to 1,3-BD selectivity. The activation energies of both products are comparable to those found in the literature for the K-ZrO-ZnO-promoted MgO/SiO₂ catalyst at 16.5 and 23 kcal/ mol, respectively. 61,62 This higher activation energy of 1,3-BD is likely due to the improved acetaldehyde activity of the catalyst, which further shifted the rate-determining step and lowered the apparent activation energy of the final product. 61,62 Importantly, the Arrhenius plot shown in the Figure 2 inset of acetaldehyde formation was not linear because of the involvement in further reactions.

The competitive reactions of dehydration and dehydrogenation were highlighted by the TPSR experiments. Although ethylene was the first vapor-phase product detected during the experiment, acetaldehyde was detected at higher temperatures, that is, >300 °C. However, 1,3-BD was detected sooner than acetaldehyde, which indicates the strong interaction between acetaldehyde and the surface. A previous investigation using DRIFTS also suggested that acetaldehyde and its surface intermediates were formed around 200 °C, lower than the formation of ethylene.²² This strong interaction between acetaldehyde and the surface was also demonstrated in Figure 3 right. The low-temperature peak, that is, 210 °C, was due to the aldol condensation between the two acetaldehyde molecules. The presence of ethanol during the experiment imposes competitive surface MPV reduction and desorption of crotonaldehyde, as previously suggested, ²² and in the absence of ethanol leads to a higher desorption rate of crotonaldehyde. The presence of crotonaldehyde was supported by the presence of m/z = 45. Alternatively, m/z can also be associated with 3-hydroxybutanal (acetaldol), which can indicate acetaldol formed on the surface during the aldol condensation.

The reverse reaction of acetaldol on the surface was also expected when ethanol was not present on the surface because it would shift the equilibrium when the resulting crotonaldehyde is not reacted. This is suggested by the relatively lower intensity of m/z = 45 between 300 and 350 °C than that of crotonaldehyde in combination with the increasing acetaldehyde signal. The sudden change in the slope of the TP (temperature-programmed) peak of m/z, that is, 44, 45, and 70, indicates an additional different reaction mechanism for aldol condensation. Palagin et al. suggested an alternative mechanism for aldol condensation without the enolization step. 64 A comparison between H-D exchange experiments of Sn-BEA, Zr-BEA, and Ti-BEA demonstrated that enolized acetaldehyde was only stabilized over Sn-BEA. A separate mechanism took place where an open Lewis-bound acetaldehyde interacted with a second acetaldehyde adsorbed on the opposing OH group of the catalyst. The DFT calculation showed that the activation energy of this second mechanism was more than triple than that of the enolization mechanism (\sim 2 eV vs \sim 0.6 eV). ⁶⁴ A correlation can be drawn between the two classes of catalysts, largely due to the same mechanistic pathways that were observed for both MgO/SiO₂ catalysts ^{17,22} and solid Lewis acid catalysts, such as Ta₂O₅/SiO₂ and ZrO₂/ SiO₂. 5,65

The facile aldol condensation/acetaldol dehydration on the catalyst surface suggested ethanol to acetaldehyde to be the rate-limiting step. This is further supported by our TPSR experiment, when acetaldehyde was preadsorbed before temperature increase was performed under a constant ethanol flow. The 1,3-BD production onset coincided with a marked ethanol signal decline, suggesting that the MPV reduction becomes the rate-determining step when acetaldehyde/crotonaldehyde is accumulated on the surface. The increase of the acetaldehyde signal was mostly from both activated ethanol dehydrogenation and the MPV reduction byproduct because H₂ also increased at higher temperatures.

4.2. Reactive Sites on the MgSi-WK Catalyst. The LASs on MgSi-WK are fundamentally represented by the Mg atoms in four groups, Mg-O(H)-Mg, Mg-O(H)-Si, Mg-O-Mg, and Mg-O-Si, with the first two groups being the open LASs. These were further distinguished by the coordination number of the magnesium atoms: the lower the coordination, the stronger the atom is due to the electron deficiency of the cation. Our complementary bulk and surface characterization using both XRD and LEIS led to the determination of two separate bulk phases, that is, crystalline MgO and amorphous SiO₂. Although the bulk of the catalyst is dominated by the MgO crystalline phase, persistence of SiO₂ separated in an amorphous phase was also observed. HS-LEIS showed that the surface of the catalyst contains a large amount of Si atoms. Although LEIS cannot determine the configuration of the surface species, it suggests that silicate-like sites are formed. The use of ²⁹Si CP MAS NMR on similar catalysts implied that various hydrous and anhydrous magnesium silicate phases were formed. The presence of a significant amount of Si on

the surface suggests that Mg–O–Si linkages are formed. Although XRD detected separation between two phases in the bulk of the catalyst, that is, the presence of both crystalline MgO and amorphous SiO₂, HS-LEIS showed surface mixing between the two phases. As a result, the crystalline MgO phase is more dominant in the bulk, whereas the surface contains more Si, which suggested a certain amount of Mg–O–Si linkages. Collectively, these data are summarized in Figure 12, as inferred through the combination of XRD, HS-LEIS, and DRIFTS.

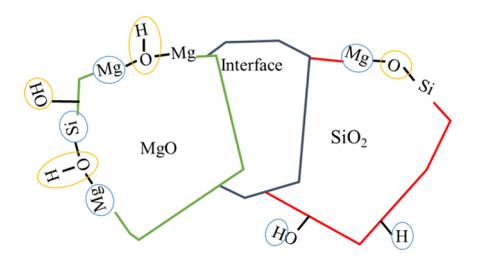


Figure 12. Schematic diagram to show the presence of various surface sites. The bulk was composed of crystalline MgO and amorphous SiO_2 , whereas the surface contained both individual oxides and silicates. The basic sites (orange) are shown in the figure as both Brønsted base (OH) and Lewis site (electron accepting oxygen atoms), and acid sites (blue) are represented as BASs (H) and LASs (electron-donating magnesium and silicon atoms).

The basic MgO sites were prevalent when the catalyst was exposed to CO₂. Assignment of these bands was based on the adsorbed carbonates and bicarbonates on Mg-O sites because CO₂ adsorption on Si sites should not yield any surface species. In $\nu_3(COO^-)$, vibration of carbonate on MgO is assigned to bidentate with ~1650 (ν_3^{as}) and ~1300 cm⁻¹ (ν_3^{s}) and monodentate carbonate ~1550 (ν_3^{as}) and ~1400 cm⁻¹ $(\nu_3^{\rm s})$, whereas bicarbonate is detected at ~1650 $(\nu_3^{\rm as})$ and $\sim 1380 \text{ cm}^{-1} (\nu_3^s)^{.57,66}$ These three species were present on the MgSi-WK catalyst, demonstrated by peaks at 1650 and ~1360 cm⁻¹ (bidentate carbonate), 1531 and ~1420 cm⁻¹ (monodentate carbonate) and ~1670, and 1405 cm⁻¹ (bicarbonate), respectively. The dominant peaks were those originating from monodentate carbonate and bicarbonate. At high temperatures, that is, 450 °C, these peaks decreased, which indicated the weakened basic sites. The intensity of these (bi)carbonate peaks decreased as the temperature was increased in the order of bicarbonate > bidentate carbonate > monodentate carbonate. Monodentate and bidentate carbonates were formed by CO2 interaction with the Mg-O Lewis acid-base pair and hence are designated as medium and strong basic sites. The easiest to desorb bicarbonate structures, on the other hand, were formed through the interaction of CO2 and the basic Mg-OH group. We did observe the appearance of negative peaks at 3740 (weak), 3725 (weak), and 3680 (very weak) cm⁻¹ when CO₂ was adsorbed on the catalyst surface at 100 °C (not shown), which suggested the consumption of the native OH group to produce surface bicarbonate. Although pyridine cannot discriminate open LASs from closed sites, combination with the CO₂ DRIFTS experiment provides more information on the molecular nature of the catalytic functional groups. The two different sites are distinguished by the consumed bicarbonate species, which is formed when CO₂ is adsorbed to a site containing the OH group. Hence, the consumption of both LASs and the bicarbonate site (weak

basic site) can be traced to the open LASs. The two open sites, that is, Mg–O(H)–Mg and Mg–O(H)–Si, were discriminated by the strength of the base pair. The former is less likely to participate during the reaction because of its very basic nature. However, activation of this group has been observed when bare MgO is activated using NH₃-thermally treated MgO.¹³ The Mg–O–Si linkages have previously been correlated with the enhanced activity, whereas open LASs had been shown to be responsible for the increased 1,3-BD production.²⁵

On pure dehydroxylated MgO, NH3 adsorbs as a physisorbed molecule, with a peak at ~1605 cm⁻¹, whereas two different LASs exhibited vibrational peaks at >1605 and 1560 cm^{-1.67,68} On the hydroxylated surface, however, the interaction is more complicated because of the contributions of OH groups, where hydrogen bonding between NH₂H-OH (1612 cm⁻¹) and H₃N-HO (1634 cm⁻¹) obscured the DRIFTS spectra. The peak at 1430 cm⁻¹ was assigned to ammonium ion (NH_4^+) as a result from interaction between ammonia and a BAS. The presence of BASs during NH_3 but not pyridine probing has been observed in the past, where pyridine underrepresented the amount of acidic sites. 9,69 This discrepancy was due to the size of the molecule with NH3 being more mobile than pyridine. The BAS that was found on the catalysts was isolated and less-accessible and hence might participate less during the reaction. Regardless, a combination of NH3 DRIFTS and DFT structural calculations allowed revealing a series of closed LAS (Mg_{3C}) as well as open LAS situated in the proximity of Mg_{4C}. Additionally, Echterhoff and Knözinger attributed a peak at 1634 cm⁻¹ to hydrogen bonding between ammonia and surface hydroxyl (NH2-H-HO-Mg).⁶⁸ This vibrational mode is entirely possible because of the identified NH₄⁺ on the surface indicating the presence of some BASs. Although DFT simulations were performed on an idealistic MgO structure, it can also be propagated to SiO₂perturbed sites. Assuming a Si atom replaces one Mg atom in the Mg_{3C}-O_{4C}-Mg_{4C} (closed LASs) and results in Mg-O-Si linkage; then, a change in electronegativity will occur, and the magnesium atom becomes more positively charged, which would result in the shorter bond between the Mg and N atoms. The shorter bond would result in the shift of the peak to a higher wavenumber, in this case higher than 1620 cm⁻¹.

A combination of experiments used to elucidate the reactive sites of the catalyst indicated that there were two prominent sites involved during the experiment. The OH groups were doubly coordinated to a Mg and a Si atom and the very reactive Lewis acid-base pair was coordinated in the form of Mg-O-Mg or Mg-O-Si. From CO₂ and NH₃ poisoning experiments, it can be inferred that the OH groups acted as a weak basic site as well as were involved in the formation of an open LAS. These sites were responsible during the catalytic reactions of ethanol via both the aldol mechanism and ethanol dehydration to ethylene.

5. CONCLUSIONS

The molecular structure and reactivity of the MgO/SiO₂ catalyst, prepared using wet kneading, active surface sites were analyzed using in situ DRIFTS (using complementary DFT calculations), TPSR–MS, and steady-state reactions in combination with bulk XRD and surface LEIS measurements. The MgSi-WK surface contained a significant number of surface sites derived from magnesium silicates as indicated by the distinct OH groups in DRIFTS spectra. Although XRD

indicated the presence of crystalline MgO and some amorphous SiO2, surface LEIS analysis showed high Si concentration. Using reactive molecule surface site poisoning experiments, it was determined that the weak basic sites were responsible for ethanol dehydrogenation and strong basic sites were responsible for aldol condensation and MPV reduction, whereas stronger acid sites catalyzed acetaldol and crotyl alcohol dehydration reactions and weak acid sites catalyzed the undesired ethanol dehydration. Furthermore, through a combination of NH₃-TPD and DFT calculations, the presence of open and closed LASs was suggested. The MgSi-WK catalyst was shown to have both open LASs with both Mg_{3C} and Mg_{4C} as the anchoring LASs and also a very isolated closed LAS (Mg_{3C} and Mg_{4C}). In situ DRIFT and fixed-bed measurements indicated the consumption of the weak basic sites during the catalytic reaction. These weak basic sites resulted from MgO/SiO2-OH. LASs were also consumed during the adsorption and the reaction and no generation of the new BASs was observed.

AUTHOR INFORMATION

Corresponding Author

*E-mail: job314@lehigh.edu. Phone +1-610-758-6836.

ORCID ®

Jonas Baltrusaitis: 0000-0001-5634-955X

Notes

The authors declare no competing financial interest.

ACKNOWLEDGMENTS

This work was supported by National Science Foundation under grant no. CHE 1710120. The authors gratefully acknowledge Prof. Israel E. Wachs for access to their TPSR—MS instrument. Lehigh University Professor John C. Chen Fellowship and P.C. Rossin Professorship are acknowledged. This work used the Extreme Science and Engineering Discovery Environment (XSEDE),⁷⁰ which is supported by the National Science Foundation grant number ACI-1053575.

REFERENCES

- (1) Chung, S.-H.; Angelici, C.; Hinterding, S. O. M.; Weingarth, M.; Baldus, M.; Houben, K.; Weckhuysen, B. M.; Bruijnincx, P. C. A. Role of Magnesium Silicates in Wet-Kneaded Silica-Magnesia Catalysts for the Lebedev Ethanol-to- Butadiene Process. *ACS Catal.* **2016**, *6*, 4034–4045.
- (2) Velasquez Ochoa, J.; Bandinelli, C.; Vozniuk, O.; Chieregato, A.; Malmusi, A.; Recchi, C.; Cavani, F. An Analysis of the Chemical, Physical and Reactivity Features of MgO-SiO2 Catalysts for Butadiene Synthesis with the Lebedev Process. *Green Chem.* **2016**, 18, 1653–1663.
- (3) Shylesh, S.; Gokhale, A. A.; Scown, C. D.; Kim, D.; Ho, C. R.; Bell, A. T. From Sugars to Wheels: The Conversion of Ethanol to 1,3-Butadiene over Metal-Promoted Magnesia-Silicate Catalysts. *Chem-SusChem* **2016**, *9*, 1462–1472.
- (4) Huang, X.; Men, Y.; Wang, J.; An, W.; Wang, Y. Highly Active and Selective Binary MgO-SiO2 Catalysts for the Production of 1,3-Butadiene from Ethanol. *Catal. Sci. Technol.* **2017**, 7, 168–180.
- (5) Müller, P.; Burt, S. P.; Love, A. M.; McDermott, W. P.; Wolf, P.; Hermans, I. Mechanistic Study on the Lewis Acid Catalyzed Synthesis of 1,3-Butadiene over Ta-BEA Using Modulated Operando DRIFTS-MS. ACS Catal. 2016, 6, 6823–6832.
- (6) Sushkevich, V. L.; Ivanova, I. I.; Taarning, E. Ethanol Conversion into Butadiene over Zr-Containing Molecular Sieves Doped with Silver. *Green Chem.* **2015**, *17*, 2552–2559.

- (7) Shylesh, S.; Gokhale, A. A.; Ho, C. R.; Bell, A. T. Novel Strategies for the Production of Fuels, Lubricants, and Chemicals from Biomass. *Acc. Chem. Res.* **2017**, *50*, 2589–2597.
- (8) Pomalaza, G.; Capron, M.; Ordomsky, V.; Dumeignil, F. Recent Breakthroughs in the Conversion of Ethanol to Butadiene. *Catalysts* **2016**, *6*, 203–237.
- (9) Angelici, C.; Velthoen, M. E. Z.; Weckhuysen, B. M.; Bruijnincx, P. C. A. Influence of Acid-Base Properties on the Lebedev Ethanol-to-Butadiene Process Catalyzed by SiO2-MgO Materials. *Catal. Sci. Technol.* **2015**, *5*, 2869–2879.
- (10) He, R.; Men, Y.; Huang, X.; Wang, J.; Li, S.; Wang, X. Interaction of Ethanol with MgO-SiO2 Catalysts Studied by TPD Techniques. *Chem. Lett.* **2018**, 47, 1097–1100.
- (11) Kvisle, S.; Aguero, A.; Sneeden, R. P. A. Transformation of Ethanol into 1,3-Butadiene over Magnesium Oxide/Silica Catalysts. *Appl. Catal.* **1988**, *43*, 117–131.
- (12) Angelici, C.; Velthoen, M. E. Z.; Weckhuysen, B. M.; Bruijnincx, P. C. A. Effect of Preparation Method and CuO Promotion in the Conversion of Ethanol into 1,3-Butadiene over SiO2–MgO Catalysts. *ChemSusChem* **2014**, *7*, 2505–2515.
- (13) Hayashi, Y.; Akiyama, S.; Miyaji, A.; Sekiguchi, Y.; Sakamoto, Y.; Shiga, A.; Koyama, T.-R.; Motokura, K.; Baba, T. Experimental and Computational Studies of the Roles of MgO and Zn in Talc for the Selective Formation of 1,3-Butadiene in the Conversion of Ethanol. *Phys. Chem. Chem. Phys.* **2016**, *18*, 25191–25209.
- (14) Di Valentin, C.; Del Vitto, A.; Pacchioni, G.; Abbet, S.; Wörz, A. S.; Judai, K.; Heiz, U. Chemisorption and Reactivity of Methanol on MgO Thin Films. *J. Phys. Chem. B* **2002**, *106*, 11961–11969.
- (15) Cavalleri, M.; Pelmenschikov, A.; Morosi, G.; Gamba, A.; Coluccia, S.; Martra, G. Dissociative Adsorption of H2 on Defect Sites of MgO: A Combined IR Spectroscopic and Quantum Chemical Study. In Oxide-Based Systems at the Crossroads of Chemistry Second International Workshop, October 8–11, 2000, Como, Italy; Gamba, A., Colella, C., Coluccia, S., Eds.; Elsevier, 2001; Vol. 140, pp 131–139.
- (16) Branda, M. M.; Rodríguez, A. H.; Belelli, P. G.; Castellani, N. J. Ethanol Adsorption on MgO Surface with and without Defects from a Theoretical Point of View. *Surf. Sci.* **2009**, *603*, 1093–1098.
- (17) Taifan, W. E.; Bučko, T.; Baltrusaitis, J. Catalytic Conversion of Ethanol to 1,3-Butadiene on MgO: A Comprehensive Mechanism Elucidation Using DFT Calculations. *J. Catal.* **2017**, *346*, 78–91.
- (18) Chieregato, A.; Velasquez Ochoa, J.; Bandinelli, C.; Fornasari, G.; Cavani, F.; Mella, M. On the Chemistry of Ethanol on Basic Oxides: Revising Mechanisms and Intermediates in the Lebedev and Guerbet Reactions. *ChemSusChem* **2014**, *8*, 377–388.
- (19) Fan, D.; Dong, X.; Yu, Y.; Zhang, M. A DFT Study on the Aldol Condensation Reaction on MgO in the Process of Ethanol to 1,3-Butadiene: Understanding the Structure-Activity Relationship. *Phys. Chem. Chem. Phys.* **2017**, *19*, 25671–25682.
- (20) Janssens, W.; Makshina, E. V.; Vanelderen, P.; De Clippel, F.; Houthoofd, K.; Kerkhofs, S.; Martens, J. A.; Jacobs, P. A.; Sels, B. F. Ternary Ag/MgO-SiO2 Catalysts for the Conversion of Ethanol into Butadiene. *ChemSusChem* **2014**, *8*, 994–1008.
- (21) Larina, O. V.; Kyriienko, P. I.; Trachevskii, V. V.; Vlasenko, N. V.; Soloviev, S. O. Effect of Mechanochemical Treatment on Acidic and Catalytic Properties of MgO-SiO2 Composition in the Conversion of Ethanol To 1,3-Butadiene. *Theor. Exp. Chem.* **2016**, *51*, 387–393.
- (22) Taifan, W. E.; Yan, G. X.; Baltrusaitis, J. Surface Chemistry of MgO/SiO2 Catalysts during the Ethanol Catalytic Conversion to 1,3-Butadiene: In Situ DRIFTS and DFT Study. *Catal. Sci. Technol.* **2017**, 7, 4648–4668.
- (23) ter Veen, H. R. J.; Kim, T.; Wachs, I. E.; Brongersma, H. H. Applications of High Sensitivity-Low Energy Ion Scattering (HS-LEIS) in Heterogeneous Catalysis. *Catal. Today* **2009**, *140*, 197–201.
- (24) Fairley, N. CasaXPS: Spectrum Processing Software for XPS, AES and SIMS, Version 2.3.13; Casa Software Ltd.: Cheshire, 2006.
- (25) Sushkevich, V. L.; Palagin, D.; Ivanova, I. I. With Open Arms: Open Sites of ZrBEA Zeolite Facilitate Selective Synthesis of Butadiene from Ethanol. *ACS Catal.* **2015**, *5*, 4833–4836.

- (26) Harris, J. W.; Cordon, M. J.; Di Iorio, J. R.; Vega-Vila, J. C.; Ribeiro, F. H.; Gounder, R. Titration and Quantification of Open and Closed Lewis Acid Sites in Sn-Beta Zeolites That Catalyze Glucose Isomerization. *J. Catal.* **2016**, 335, 141–154.
- (27) Boronat, M.; Concepcion, P.; Corma, A.; Navarro, M. T.; Renz, M.; Valencia, S. Reactivity in the Confined Spaces of Zeolites: The Interplay between Spectroscopy and Theory to Develop Structure-Activity Relationships for Catalysis. *Phys. Chem. Chem. Phys.* **2009**, *11*, 2876–2884.
- (28) Boronat, M.; Concepción, P.; Corma, A.; Renz, M.; Valencia, S. Determination of the Catalytically Active Oxidation Lewis Acid Sites in Sn-Beta Zeolites, and Their Optimisation by the Combination of Theoretical and Experimental Studies. *J. Catal.* **2005**, 234, 111–118.
- (29) Kantorovich, L. N.; Holender, J. M.; Gillan, M. J. The Energetics and Electronic Structure of Defective and Irregular Surfaces on MgO. *Surf. Sci.* **1995**, 343, 221–239.
- (30) Chizallet, C.; Petitjean, H.; Costentin, G.; Lauron-Pernot, H.; Maquet, J.; Bonhomme, C.; Che, M. Identification of the OH Groups Responsible for Kinetic Basicity on MgO Surfaces by 1H MAS NMR. *J. Catal.* **2009**, 268, 175–179.
- (31) Chizallet, C.; Costentin, G.; Che, M.; Delbecq, F.; Sautet, P. Infrared Characterization of Hydroxyl Groups on MgO: A Periodic and Cluster Density Functional Theory Study Infrared Characterization of Hydroxyl Groups on MgO: A Periodic and Cluster Density Functional Theory Study. J. Am. Chem. Soc. 2007, 129, 6442–6452.
- (32) Chizallet, C.; Costentin, G.; Che, M.; Delbecq, F.; Sautet, P. Revisiting Acido-Basicity of the MgO Surface by Periodic Density Functional Theory Calculations: Role of Surface Topology and Ion Coordination on Water Dissociation. *J. Phys. Chem. B* **2006**, *110*, 15878–15886.
- (33) Sushko, P. V.; Shluger, A. L.; Catlow, C. R. A. Relative Energies of Surface and Defect States: Ab Initio Calculations for the MgO (001) Surface. *Surf. Sci.* **2000**, *450*, 153–170.
- (34) Bailly, M.; Chizallet, C.; Costentin, G.; Krafft, J.; Lauronpernot, H.; Che, M. A Spectroscopy and Catalysis Study of the Nature of Active Sites of MgO Catalysts: Thermodynamic Brønsted Basicity versus Reactivity of Basic Sites. *J. Catal.* **2005**, 235, 413–422.
- (35) Chizallet, C.; Bailly, M. L.; Costentin, G.; Lauron-Pernot, H.; Krafft, J. M.; Bazin, P.; Saussey, J.; Che, M. Thermodynamic Brønsted Basicity of Clean MgO Surfaces Determined by Their Deprotonation Ability: Role of Mg2+-O2- Pairs. *Catal. Today* **2006**, *116*, 196–205.
- (36) Baltrusaitis, J.; Hatch, C.; Orlando, R. Periodic DFT Study of Acidic Trace Atmospheric Gas Molecule Adsorption on Ca- and Fe-Doped MgO(001) Surface Basic Sites. *J. Phys. Chem. A* **2012**, *116*, 7950–7958.
- (37) Haas, P.; Tran, F.; Blaha, P. Calculation of the Lattice Constant of Solids with Semilocal Functionals. *Phys. Rev. B: Condens. Matter Mater. Phys.* **2009**, *79*, 085104.
- (38) Kresse, G.; Hafner, J. Ab Initio Molecular-Dynamics Simulation of the Liquid-Metal Amorphous-Semiconductor Transition in Germanium. *Phys. Rev. B: Condens. Matter Mater. Phys.* **1994**, 49, 14251–14269.
- (39) Kresse, G.; Furthmüller, J. Efficiency of Ab-Initio Total Energy Calculations for Metals and Semiconductors Using a Plane-Wave Basis Set. *Comput. Mater. Sci.* **1996**, *6*, 15–50.
- (40) Kresse, G.; Furthmüller, J. Efficient Iterative Schemes for Ab Initio Total-Energy Calculations Using a Plane-Wave Basis Set. *Phys. Rev. B: Condens. Matter Mater. Phys.* **1996**, *54*, 11169–11186.
- (41) Kresse, G.; Hafner, J. Ab Initio Molecular Dynamics for Open-Shell Transition Metals. *Phys. Rev. B: Condens. Matter Mater. Phys.* **1993**, 48, 13115–13118.
- (42) Blöchl, P. E. Projector Augmented-Wave Method. *Phys. Rev. B: Condens. Matter Mater. Phys.* **1994**, *50*, 17953–17979.
- (43) Perdew, J. P.; Burke, K.; Ernzerhof, M. Generalized Gradient Approximation Made Simple. *Phys. Rev. Lett.* **1996**, *77*, 3865–3868.
- (44) Golay, S.; Kiwi-Minsker, L.; Doepper, R.; Renken, A. Influence of the Catalyst Acid/Base Properties on the Catalytic Ethanol Dehydration under Steady State and Dynamic Conditions. In Situ

- Surface and Gas-Phase Analysis. Chem. Eng. Sci. 1999, 54, 3593–3598.
- (45) Di Cosimo, J. I.; Díez, V. K.; Xu, M.; Iglesia, E.; Apesteguía, C. R. Structure and Surface and Catalytic Properties of Mg-Al Basic Oxides. *J. Catal.* **1998**, *178*, 499–510.
- (46) Phung, T. K.; Busca, G. Ethanol Dehydration on Silica-Aluminas: Active Sites and Ethylene/Diethyl Ether Selectivities. *Catal. Commun.* **2015**, *68*, 110–115.
- (47) Ordomsky, V. V.; Sushkevich, V. L.; Ivanova, I. I. Study of Acetaldehyde Condensation Chemistry over Magnesia and Zirconia Supported on Silica. *J. Mol. Catal. A: Chem.* **2010**, 333, 85–93.
- (48) Davydov, A. Molecular Spectroscopy of Oxide Catalyst Surfaces; John Wiley & Sons Ltd: West Sussex PO19 8SQ, England, 2003.
- (49) Keturakis, C. Operando Molecular Spectroscopy during Catalytic Biomass Pyrolysis; Lehigh University, 2015.
- (50) Knözinger, E.; Jacob, K.-H.; Singh, S.; Hofmann, P. Hydroxyl Groups as IR Active Surface Probes on MgO Crystallites. *Surf. Sci.* **1993**, 290, 388–402.
- (51) Bian, S.-W.; Baltrusaitis, J.; Galhotra, P.; Grassian, V. H. A Template-Free, Thermal Decomposition Method to Synthesize Mesoporous MgO with a Nanocrystalline Framework and Its Application in Carbon Dioxide Adsorption. *J. Mater. Chem.* **2010**, 20, 8705–8710.
- (52) Lercher, J. A.; Grijndling, C.; Eder-Mirth, G. Infrared Studies of the Surface Acidity of Oxides and Zeolites Using Adsorbed Probe Molecules. *Catal. Today* **1996**, *27*, 353–376.
- (53) Lavalley, J. C. Infrared Studies of the Surface Basicity of Metal Oxides and Zeolites Using Adsorbed Probe Molecules. *Catal. Today* **1996**, 27, 377–401.
- (54) Vimont, A.; Thibault-Starzyk, F.; Daturi, M. Analysing and Understanding the Active Site by IR Spectroscopy. *Chem. Soc. Rev.* **2010**, 39, 4928–4950.
- (55) Busch, O. M.; Brijoux, W.; Thomson, S.; Schüth, F. Spatially Resolving Infrared Spectroscopy for Parallelized Characterization of Acid Sites of Catalysts via Pyridine Sorption: Possibilities and Limitations. *J. Catal.* **2004**, 222, 174–179.
- (56) Tamura, M.; Shimizu, K.-i.; Satsuma, A. Comprehensive IR Study on Acid/Base Properties of Metal Oxides. *Appl. Catal., A* **2012**, 433–434, 135–145.
- (57) Busca, G.; Lorenzelli, V. Infrared Spectroscopic Identification of Species Arising from Reactive Adsorption of Carbon Oxides on Metal Oxide Surfaces. *Mater. Chem.* **1982**, *7*, 89–126.
- (58) DeWilde, J. F.; Chiang, H.; Hickman, D. A.; Ho, C. R.; Bhan, A. Kinetics and Mechanism of Ethanol Dehydration on γ -Al2O3: The Critical Role of Dimer Inhibition. *ACS Catal.* **2013**, *3*, 798–807.
- (59) Zhu, Q.; Wang, B.; Tan, T. Conversion of Ethanol and Acetaldehyde to Butadiene over MgO–SiO2 Catalysts: Effect of Reaction Parameters and Interaction between MgO and SiO2 on Catalytic Performance. ACS Sustainable Chem. Eng. 2017, 5, 722–733.
- (60) Badlani, M.; Wachs, I. E. Methanol: A "Smart" Chemical Probe Molecule. Catal. Lett. 2001, 75, 137–149.
- (61) Da Ros, S.; Jones, M. D.; Mattia, D.; Schwaab, M.; Noronha, F. B.; Pinto, J. C. Modelling the Effects of Reaction Temperature and Flow Rate on the Conversion of Ethanol to 1,3-Butadiene. *Appl. Catal., A* **2017**, 530, 37–47.
- (62) Da Ros, S.; Jones, M. D.; Mattia, D.; Pinto, J. C.; Schwaab, M.; Noronha, F. B.; Kondrat, S. A.; Clarke, T. C.; Taylor, S. H. Ethanol to 1,3-Butadiene Conversion by Using ZrZn-Containing MgO/SiO 2 Systems Prepared by Co-Precipitation and Effect of Catalyst Acidity Modification. *ChemCatChem* **2016**, *8*, 2376–2386.
- (63) Toussaint, W. J.; Dunn, J. T.; Jachson, D. R. Production of Butadiene from Alcohol. *Ind. Eng. Chem.* **1947**, *39*, 120–125.
- (64) Palagin, D.; Sushkevich, V. L.; Ivanova, I. I. C-C Coupling Catalyzed by Zeolites: Is Enolization the Only Possible Pathway for Aldol Condensation? *J. Phys. Chem. C* **2016**, *120*, 23566–23575.
- (65) Sushkevich, V. L.; Ivanova, I. I. Mechanistic Study of Ethanol Conversion into Butadiene over Silver Promoted Zirconia Catalysts. *Appl. Catal., B* **2017**, *215*, 36–49.

- (66) Taifan, W.; Boily, J.-F.; Baltrusaitis, J. Surface Chemistry of Carbon Dioxide Revisited. Surf. Sci. Rep. 2016, 71, 595–671.
- (67) Echterhoff, R.; Knözinger, E. FT-IR Characterization of Adsorption Complexes on Magnesium Oxide Surfaces. *J. Mol. Struct.* **1988**, *174*, 343–350.
- (68) Echterhoff, R.; Knözinger, E. FTIR Spectroscopic Characterization of the Adsorption and Desorption of Ammonia on MgO Surfaces. *Surf. Sci.* **1990**, 230, 237–244.
- (69) Angelici, C.; Meirer, F.; van der Eerden, A. M. J.; Schaink, H. L.; Goryachev, A.; Hofmann, J. P.; Hensen, E. J. M.; Weckhuysen, B. M.; Bruijnincx, P. C. A. Ex Situ and Operando Studies on the Role of Copper in Cu-Promoted SiO2–MgO Catalysts for the Lebedev Ethanol-to-Butadiene Process. ACS Catal. 2015, 5, 6005–6015.
- (70) Towns, J.; Cockerill, T.; Dahan, M.; Foster, I.; Gaither, K.; Grimshaw, A.; Hazlewood, V.; Lathrop, S.; Lifka, D.; Peterson, G. D.; et al. XSEDE: Accelerating Scientific Discovery. *Comput. Sci. Eng.* **2014**, *16*, 62–74.